

# Morphology–elasticity relationships using decreasing fabric information of human trabecular bone from three major anatomical locations

Thomas Gross · Dieter H. Pahr · Philippe K. Zysset

Received: 3 May 2012 / Accepted: 18 September 2012 / Published online: 2 October 2012  
© Springer-Verlag Berlin Heidelberg 2012

**Abstract** With improving clinical CT scanning technology, the accuracy of CT-based finite element (FE) models of the human skeleton may be ameliorated by an enhanced description of apparent level bone mechanical properties. Micro-finite element ( $\mu$ FE) modeling can be used to study the apparent elastic behavior of human cancellous bone. In this study, samples from the femur, radius and vertebral body were investigated to evaluate the predictive power of morphology–elasticity relationships and to compare them across different anatomical regions.  $\mu$ FE models of 701 trabecular bone cubes with a side length of 5.3 mm were analyzed using kinematic boundary conditions. Based on the FE results, four morphology–elasticity models using bone volume fraction as well as full, limited or no fabric information were calibrated for each anatomical region. The 5 parameter Zysset–Curnier model using full fabric information showed excellent predictive power with coefficients of determination ( $r_{\text{adj}}^2$ ) of 0.98, 0.95 and 0.94 of the femur, radius and vertebra data, respectively, with mean total norm errors between 14 and 20 %. A constant orthotropy model and a constant transverse isotropy model, where the elastic anisotropy is defined by the model parameters, yielded coefficients of determination between 0.90 and 0.98 with total norm errors between 16 and 25 %. Neglecting fabric information and using an isotropic model led to  $r_{\text{adj}}^2$  between 0.73 and 0.92 with total norm errors between 38 and 49 %. A comparison of the model regressions revealed minor but significant ( $p < 0.01$ ) differ-

ences for the fabric–elasticity model parameters calibrated for the different anatomical regions. The proposed models and identified parameters can be used in future studies to compute the apparent elastic properties of human cancellous bone for homogenized FE models.

**Keywords** Elasticity · Fabric · Mechanical properties · Finite element method · Human cancellous bone

## 1 Introduction

Finite element (FE) modeling is becoming increasingly popular as a tool to predict mechanical loading responses of full bones (Cristofolini et al. 2010; Jones and Wilcox 2008; Taddei et al. 2006), bone segments (Varga et al. 2011; Silva et al. 1998) and bone implant systems (Bougherara et al. 2010; Roychowdhury 2009) in humans. However, all macro-level FE models rely on homogenized material properties of trabecular bone, in which determination is a delicate task.

Ex vivo, the fabric information can be accurately assessed by means of high-resolution CT images, and homogenized bone FE models using fabric-based orthotropic material behavior have shown better predictions of stiffness and strength than models using bone volume fraction alone (Pahr and Zysset 2009). Up to date, clinical FE models of the central skeleton use either isotropic symmetry (Keyak et al. 2011) or in case of the vertebral body transverse isotropic symmetry where the direction of anisotropy is based on anatomical considerations (Chevalier et al. 2010). However, with improving CT scanning technology (Mulder et al. 2012) and advanced image processing algorithms (Graeff et al. 2007), it is now possible to also analyze the trabecular bone structure in vivo. This opens the opportunity to include location-specific

T. Gross (✉) · D. H. Pahr  
Institute of Lightweight Design and Structural Biomechanics,  
Vienna University of Technology, Vienna 1040, Austria  
e-mail: tgross@ilsb.tuwien.ac.at

P. K. Zysset  
Institute for Surgical Technology and Biomechanics,  
University of Bern, Bern 3014, Switzerland

anisotropic mechanical properties as model input for clinical FE models.

Apparent mechanical properties of trabecular bone can be investigated by means of mechanical testing (Goulet et al. 1994), ultrasound wave propagation (Turner et al. 1990) and the digital finite element method (Hollister 1994). However, all of the aforementioned testing strategies struggle with either the anisotropy of cancellous bone; the fact that the characteristic length of the intratrabecular spacing is of the same order of magnitude as the characteristic length of architectural heterogeneity (Harrigan et al. 1988) or that they are only valid for a given set of boundary conditions (Pahr and Zysset 2008).

Since the apparent elastic behavior of cancellous bone is closely related to its intrinsic architecture (Cowin 1985), apparent mechanical properties can be approximated using morphological parameters which are accessible by a number of imaging techniques. Bone volume fraction ( $\rho$ ) and architectural anisotropy described by the fabric tensor ( $\mathbf{M}$ ) (Cowin 1985) can be accurately investigated using serial reconstruction (Odgaard et al. 1990), micro-computed tomography ( $\mu$ CT) (Ruegsegger et al. 1996) and micro-magnetic resonance imaging ( $\mu$ MRI) (Hipp et al. 1996).

For apparent level compression, tension and torsion tests, micro-finite element ( $\mu$ FE) models of trabecular bone which are based on high-resolution scans have shown fair to excellent agreement with mechanical tests (Wolfram et al. 2010; Chevalier et al. 2007). Unlike experimental methods,  $\mu$ FE methods for homogenization allow to compute the full anisotropic stiffness tensor of the bone microstructure.

In Zysset (2003), different testing techniques have been reviewed and models relating trabecular bone stiffness and morphology have been introduced. However, for usage in clinical FE models, the problem arises that the resolution in clinical scans is inferior to  $\mu$ CT scans and in most cases a computation of the complete fabric tensor is not possible.

Therefore, the objective of this study was to calibrate different fabric–elasticity models that are based on full, limited or no fabric information using a large data set ( $n = 701$ ) of trabecular bone cubes from the femur, radius and vertebra. Furthermore, the fabric–elasticity relationships should be established and compared across the different anatomical sites.

## 2 Theoretical models

In this study, four different models are used to relate bone volume fraction and in three cases bone volume fraction and fabric information to elastic properties obtained by  $\mu$ FE analysis. The positive definite second-order fabric tensor  $\mathbf{M}$  with the strictly positive definite eigenvalues  $m_i$  and the normalized eigenvectors  $\mathbf{m}_i$  is defined by Cowin (1985):

$$\mathbf{M} = \sum_{i=1}^3 m_i \mathbf{M}_i = \sum_{i=1}^3 m_i (\mathbf{m}_i \otimes \mathbf{m}_i), \quad (1)$$

$$m_1 \leq m_2 \leq m_3.$$

The fabric tensor  $\mathbf{M}$  is normalized by dividing it by its trace and multiplying it by a factor of 3 such that

$$\text{tr}(\mathbf{M}) = 3. \quad (2)$$

The following theoretical models were used to fit the results of the FE analyses:

### 2.1 Volume fraction and fabric-based orthotropic model (Zysset–Curnier model)

In the case of complete fabric information, the stiffness tensor ( $\mathbb{C}$ ) can be expressed by means of the five parameter Zysset–Curnier model (Zysset 2003):

$$\begin{aligned} \mathbb{C}(\rho, \mathbf{M}) = & \sum_{i=1}^3 (\lambda_0 + 2\mu_0) \rho^k m_i^{2l} \mathbf{M}_i \otimes \mathbf{M}_i \\ & + \sum_{\substack{i,j=1 \\ i \neq j}}^3 \lambda'_0 \rho^k m_i^l m_j^l \mathbf{M}_i \otimes \mathbf{M}_j \\ & + \sum_{\substack{i,j=1 \\ i \neq j}}^3 2\mu_0 \rho^k m_i^l m_j^l \mathbf{M}_i \underline{\otimes} \mathbf{M}_j. \end{aligned} \quad (3)$$

The double tensorial product of second-order tensors is defined by Curnier et al. (1994):

$$\mathbf{A} \underline{\otimes} \mathbf{B} = \frac{1}{2} (A_{ik} B_{jl} + A_{il} B_{jk}) \mathbf{e}_i \otimes \mathbf{e}_j \otimes \mathbf{e}_k \otimes \mathbf{e}_l. \quad (4)$$

### 2.2 Volume fraction and fabric-based constant orthotropic model (constant orthotropy model)

If only the three eigenvectors and the ranking of the eigenvalues ( $m_1 \geq m_2 \geq m_3$ ) of the fabric tensor are known, a constant orthotropy model with 10 constants can be used to relate bone volume fraction and limited fabric information to bone stiffness. Using this model, the stiffness tensor can be written as:

$$\begin{aligned} \mathbb{C}(\rho, \mathbf{M}_1, \mathbf{M}_2, \mathbf{M}_3) = & \sum_{i=1}^3 \lambda_{0ii} \rho^k \mathbf{M}_i \otimes \mathbf{M}_i \\ & + \sum_{\substack{i,j=1 \\ i \neq j}}^3 \lambda_{0ij} \rho^k \mathbf{M}_i \otimes \mathbf{M}_j \\ & + \sum_{\substack{i,j=1 \\ i \neq j}}^3 2\mu_{0ij} \rho^k \mathbf{M}_i \underline{\otimes} \mathbf{M}_j, \end{aligned} \quad (5)$$

$$\lambda_{0ij} = \lambda_{0ji}, \quad \mu_{0ij} = \mu_{0ji}.$$

### 2.3 Volume fraction and fabric-based constant transverse isotropic model (constant transverse isotropy model)

For bone regions, with information about the bone volume fraction and the main direction ( $\mathbf{m}_3$ ) only, a transverse isotropic approach can be used. The stiffness tensor of the constant transverse isotropy model with 6 parameters writes the following:

$$\begin{aligned} \mathbb{C}(\rho, \mathbf{M}_3) = & \lambda_0 \rho^k \mathbf{I} \otimes \mathbf{I} + 2\mu_0 \rho^k \mathbf{I} \underline{\otimes} \mathbf{I} \\ & + (\lambda_{03} - \lambda_0) \rho^k (\mathbf{I} \otimes \mathbf{M}_3 + \mathbf{M}_3 \otimes \mathbf{I}) \\ & + (\lambda_{033} + \lambda_0 - 2\lambda_{03}) \rho^k \mathbf{M}_3 \otimes \mathbf{M}_3 \\ & + (2\mu_{03} - 2\mu_0) \rho^k (\mathbf{M}_3 \underline{\otimes} \mathbf{I} + \mathbf{I} \underline{\otimes} \mathbf{M}_3) \\ & - (4\mu_{03} - 2\mu_0) \rho^k \mathbf{M}_3 \underline{\otimes} \mathbf{M}_3. \end{aligned} \quad (6)$$

### 2.4 Volume fraction-based isotropic model (isotropic model)

For no fabric information, an isotropic power model relating volume fraction and elastic properties was formulated by Gibson (1985). In this case, the isotropic stiffness tensor writes the following:

$$\mathbb{C}(\rho) = \lambda_0 \rho^k \mathbf{I} \otimes \mathbf{I} + 2\mu_0 \rho^k \mathbf{I} \underline{\otimes} \mathbf{I}. \quad (7)$$

## 3 Materials and methods

Trabecular bone sections were obtained from 3 proximal femora (3 female, age 62–75 years, mean age  $66 \pm 8$  years), 6 distal radii (three left and three right, age and gender unknown) and 6 vertebral bodies, locations L2–L4 and T11 (6 male, age 44–82, mean age  $60 \pm 16$  years). The femoral trabecular bone was extracted from the greater trochanter, lesser trochanter, femoral head and femoral neck. All sections were submerged into 0.9% saline solution and after removal of air bubbles, scanned with CT ( $\mu$ CT 40, SCANCO Medical AG, Brüttisellen, Switzerland) using the settings of 70 kVp, 114 mA, 200 ms integration time,  $2,048 \times 2,048$  pixels image matrix and  $18 \mu\text{m}$  isotropic spatial resolution. After applying a Gaussian filter ( $\sigma = 1.2$ , support = 2), cubic subregions with a side length of 5.3 mm were extracted from the  $\mu$ CT scans and further used for the analysis. For each anatomical region, an optimal threshold was computed by thresholding the individual bone cubes using the single-level threshold of IPL (SCANCO Medical AG, Brüttisellen, Switzerland) and averaging the threshold values for each region. After segmentation, unconnected bone regions were removed from the scans, bone volume fraction was computed via voxel counting, and fabric was measured using the mean intercept length (MIL) method (Whitehouse 1974) providing the fabric tensor.  $\mu$ FE models of the segmented trabecular bone cubes were created by converting image voxels into linear isotropic

eight-node hexahedral finite elements. Each element was assigned a Young's modulus of 12 GPa and a Poisson's ratio of 0.3 (Zysset et al. 1999; Wolfram et al. 2010). The apparent elastic properties of the  $\mu$ FE models were evaluated by performing FE simulations of six independent load cases under kinematic boundary conditions (Pahr and Zysset 2008). Testing of the  $\mu$ FE models comprised three compressive and three shear tests in which a linear transformation is applied to the surface nodes of the cube. The FE simulations were performed on a parallel Linux server with  $2 \times 6$  Xeon X5680 CPUs and 144 GB user memory using ParFE (2008). The full elastic stiffness tensor of each bone cube was computed by means of stress and strain averages of the FE results. Subsequently, the anisotropic stiffness tensor was rotated such that its principal directions corresponded to the fabric eigensystem leading to the rotated anisotropic stiffness tensor  $\mathbb{C}_{FE\text{aniso}}$ . In this coordinate system, an orthotropic representation  $\mathbb{C}_{FE\text{ortho}}$  was obtained by neglecting the non-orthotropic entries of the stiffness tensor (see Fig. 1). The error associated with this procedure was quantified by  $NE_{FE\text{ortho}}$  and computed by

$$NE_{FE\text{ortho}} = \frac{\|(\mathbb{C}_{FE\text{aniso}} - \mathbb{C}_{FE\text{ortho}})\|}{\|\mathbb{C}_{FE\text{aniso}}\|}. \quad (8)$$

Nonlinear optimization routines (Python, 2.6.6) were used to fit the data sets of the three anatomical regions and the combined data set (see Table 1) to the above described theoretical models (see Sect. 2). Linear regression analyses in log scale were performed between the stiffness tensors obtained from morphology–elasticity relationships ( $\mathbb{C}_{\text{aniso}}$ ) and from the FE analyses ( $\mathbb{C}_{FE\text{ortho}}$ ). The linear regression data were then studied by ANCOVA (significance level  $p < 0.01$ ) in MATLAB (Mathworks, Natick, USA) to investigate differences in the fabric–elasticity relationships between the different anatomical regions. The model norm error, expressing the variation of the model stiffness to the orthotropic FE stiffness, was computed with:

$$NE_{\text{model}} = \frac{\|(\mathbb{C}_{FE\text{ortho}} - \mathbb{C}_{\text{model}})\|}{\|\mathbb{C}_{FE\text{ortho}}\|}. \quad (9)$$

The total norm error, describing the variation of the model stiffness with respect to the full anisotropic stiffness tensor, was computed with:

$$NE_{\text{aniso}} = \frac{\|(\mathbb{C}_{FE\text{aniso}} - \mathbb{C}_{\text{model}})\|}{\|\mathbb{C}_{FE\text{aniso}}\|}. \quad (10)$$

## 4 Results

For the trabecular bone cubes from the femur, radius and vertebra, the mean bone volume fraction ( $\pm$  standard deviation) was 18.75% ( $\pm 11.56$ ), 16.45% ( $\pm 3.89$ ) and 11.32% ( $\pm 4.01$ ), the degree of anisotropy ( $\pm$  standard deviation) was

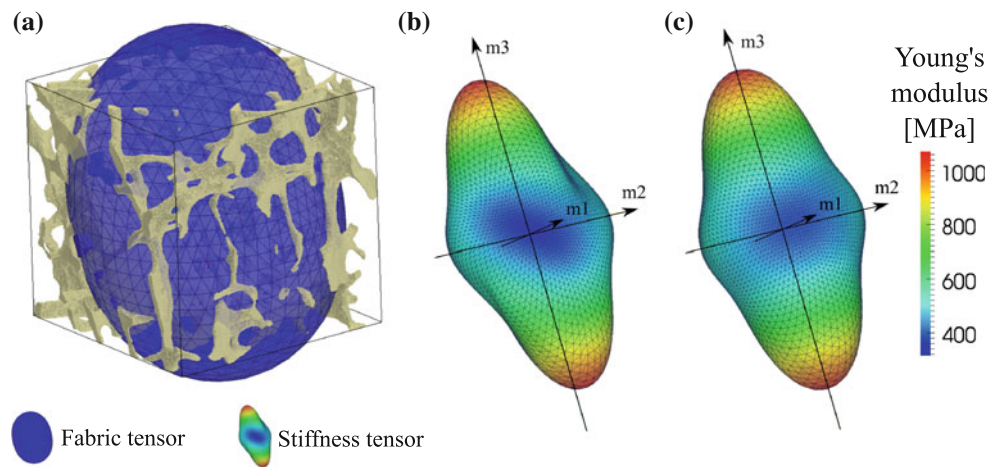


**Fig. 1** **a** Voxel model of trabecular bone cube with fabric tensor representation; **b** full anisotropic stiffness tensor in the fabric coordinate system; **c** orthotropic stiffness tensor in the fabric coordinate system

**Table 1** Descriptive statistics of the investigated bone specimens

Location	$\rho$	DA	Specimens
Femur	0.19 ( $\pm 0.10$ )	1.67 ( $\pm 0.34$ )	264
Radius	0.16 ( $\pm 0.04$ )	1.71 ( $\pm 0.23$ )	81
Vertebra	0.11 ( $\pm 0.04$ )	1.45 ( $\pm 0.20$ )	356
Combined	0.15 ( $\pm 0.084$ )	1.57 ( $\pm 0.28$ )	701

Mean values ( $\pm$  standard deviations);  $\rho$ , bone volume fraction; DA, degree of anisotropy.

1.67 ( $\pm 0.34$ ), 1.71 ( $\pm 0.23$ ) and 1.45 ( $\pm 0.20$ ) (see Table 1). In the vertebra, the mean bone volume fraction and the degree of anisotropy were significantly lower as in the femur and radius ( $p < 0.05$ ). No significant difference was found between the femur and radius for volume fraction ( $p = 0.08$ ) and DA ( $p = 0.37$ ).

The orthotropic representations of the obtained anisotropic stiffness tensors in the fabric coordinate systems of the bone cubes were associated with norm errors ( $NE_{FE_{ortho}}$ ) of 8.6% ( $\pm 0.05$ ), 4.6% ( $\pm 0.02$ ) and 7.2% ( $\pm 0.04$ ) for the femur, radius and vertebra data set.

The Zysset–Curnier model with 5 parameters and complete fabric information showed the best statistical power with coefficients of determination ( $r_{adj}^2$ ) of 0.98, 0.95 and 0.95 for the femur, radius and vertebra and a mean model norm error of 15%. The constant orthotropy model with 10 parameters and information about the principal directions of the fabric tensor led to  $r_{adj}^2$  between 0.94 and 0.98 with a mean model norm error of 18%. The constant transverse isotropy model using 6 parameters and information about the main direction of the bone regions yielded  $r_{adj}^2$  between 0.90 and 0.96 with a mean model norm error of 21%. Negligence of fabric information and the usage of an isotropic power model with 3 constants led to  $r_{adj}^2$  between 0.73 and 0.92 with a mean model norm error of 43%.

The calculated model constants and adjusted coefficients of determination of all theoretical models are shown in Table 2. The computed stiffness tensors were positive definite for all models and regions. The quality of the regressions of the Zysset–Curnier model is shown in Fig. 2.

Comparison of the model regressions using anatomy-specific parameters and the parameters from the combined data set showed a significant ( $p < 0.01$ ) difference for all anatomical regions (see Fig. 2). However, the total norm errors from the models ( $NE_{aniso}$ ) using the combined parameters were on average only 7.57% higher than the errors from the models using the anatomy-specific parameters with a relative increase in the error of 10.39, 7.32 and 5.83% for the femur, radius and vertebra.

## 5 Discussion

In this study, a data set of 701 trabecular bone cubes from the proximal femur, distal radius and lumbar and thoracic vertebra was used to study different models relating bone morphology and elastic properties. To account for situations where fabric information can not be assessed completely (clinical CT scans), models for complete, limited and no fabric information were investigated.

Bone volume fraction and degree of anisotropy from the analyzed trabecular bone regions were in the expected range and are similar to those found in Hildebrand et al. (1999); Varga and Zysset (2009); Charlebois et al. (2010). To distinguish between the different regions, analyses were performed separately for the femur, radius and vertebra data set. A combined data set consisting of the three regions and accounting for the different number of specimens in each group was also analyzed.

The apparent elastic properties of the trabecular bone cubes were computed using high-resolution digital finite

**Table 2** Model parameters and adjusted coefficients of determination in fitting the components of the three anatomical locations using different models

Location	$\lambda_0$	$\lambda'_{00}$	$\mu_0$	$k$	$l$	adj. $r^2$	$NE_{model}$ (%)	$NE_{aniso}$ (%)					
<i>(a) Zysset–Curnier model</i>													
Femur	4609.2	3691.6	3738.2	1.60	0.99	0.981	13.6	16.4					
Radius	5789.8	4068.9	4051.5	1.77	1.18	0.955	12.8	13.7					
Vertebra	6878.6	4364.2	4155.9	1.71	1.12	0.945	18.8	20.4					
Combined	4982.4	3518.5	3470.7	1.62	1.10	0.960	16.7	18.3					
Location	$\lambda_{011}$	$\lambda_{022}$	$\lambda_{033}$	$\lambda_{023}$	$\lambda_{031}$	$\lambda_{012}$	$\mu_{023}$	$\mu_{031}$	$\mu_{012}$	$k$	adj. $r^2$	$NE_{model}$ (%)	$NE_{aniso}$ (%)
<i>(b) Constant orthotropy model</i>													
Femur	6923.8	11456.5	19898.6	4549.1	3177.1	3112.4	5093.9	3294.1	2783.6	1.61	0.976	17.3	19.8
Radius	7434.4	12188.2	29500.6	5104.6	3911.6	3363.5	5936.6	4004.0	2790.7	1.80	0.940	14.7	15.6
Vertebra	9751.6	13892.0	28985.8	4869.8	4327.7	4416.3	5540.1	4321.8	3358.8	1.74	0.948	21.7	23.1
Combined	6657.0	10446.3	21480.7	4039.1	3153.5	2992.6	4602.4	3210.5	2481.9	1.63	0.951	19.1	20.1
Location	$\lambda_0$	$\lambda_{03}$	$\lambda_{033}$	$\mu_0$	$k$	adj. $r^2$	$NE_{model}$ (%)	$NE_{aniso}$ (%)					
<i>(c) Constant transverse isotropy model</i>													
Femur	3127.0	3801.7	19898.6	2831.3	4096.3	1.61	0.956	24.2					
Radius	3405.0	4469.8	29502.2	2907.45	4876.1	1.80	0.901	19.1					
Vertebra	4459.3	4591.6	28980.5	3457.4	4892.8	1.74	0.937	24.4					
Combined	3037.3	3581.9	21561.3	2561.05	3860.9	1.63	0.933	23.2					
Location	$\lambda_0$	$\mu_0$	$k$	adj. $r^2$	$NE_{model}$ (%)	$NE_{aniso}$ (%)							
<i>(d) Isotropic model</i>													
Femur	3586.8	3731.1	1.61	0.921	37.2	38.2							
Radius	4124.3	4296.0	1.80	0.732	48.8	49.0							
Vertebra	4624.6	4680.1	1.74	0.870	42.0	42.7							
Combined	3429.0	3536.0	1.63	0.869	43.2	43.9							

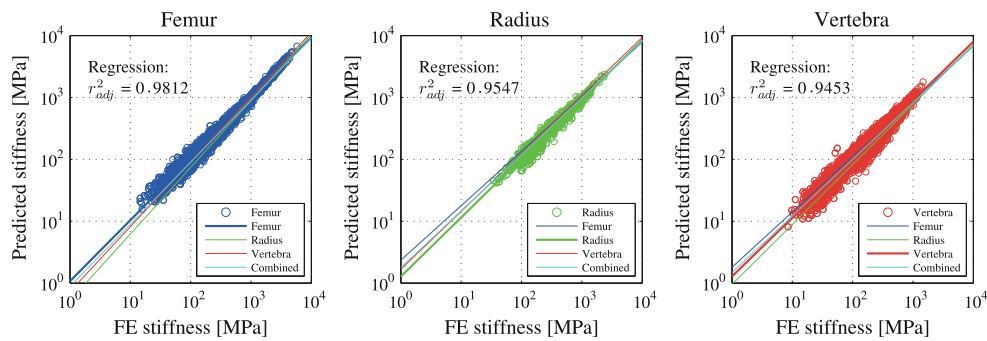


**Fig. 2** Observed ( $\mu$ FE) and computed components of the  $6 \times 6$  stiffness matrix using an orthotropic morphology–elasticity relationship. In addition, regression lines are also plotted for fabric–elasticity models with parameters calibrated with a different sample set. The FE models were based on kinematic BCs

element (micro-FE) models. This method has demonstrated fair to excellent agreement with experimental tests in the elastic loading regime (Wolfram et al. 2010; Chevalier et al. 2007).

Linear homogeneous  $\mu$ FE models of the 701 bone cubes were created using an in-house software. The tissue modulus and the Poisson’s ratio in the models were set to 12GPa and 0.3, which agrees well with material properties identified by nanoindentation and mechanical tests (Zysset et al. 1999; Wolfram et al. 2010). However, the computed model parameters can be scaled to an arbitrary tissue modulus.

In order to obtain an orthotropic representation, the computed stiffness tensors ( $\mathbb{C}_{FE_{aniso}}$ ) were rotated such that its principal directions matched the fabric eigenvectors and all the non-orthotropic entries were neglected. This approach was pursued since in homogenized FE applications, the computed model parameters will be used to build the stiffness tensor based on the fabric tensor. Therefore, it is meaningful that the stiffness tensor is also represented in the fabric coordinate system for the computation of the model parameters.

Linear regressions of the Zysset–Curnier model and the results of the FE analyses yielded coefficients of determination between 0.94 and 0.98. Using this model, the relative norm errors were 17% averaged over all regions. This is an improvement in predictive power compared to the results in Turner et al. (1990); Kabel et al. (1999); Zysset (2003) which can be attributed to the large population of specimens used in this study. The fabric–elasticity parameters found in this study are in the same range as those found in Zysset (2003) for the kinematic boundary condition-based FE results.

The constant orthotropy and the constant transverse isotropy model, where the elastic anisotropy is defined by the model parameters, also yielded high coefficients of determination with total norm errors of 20 and 23%, respectively. In cases where complete fabric information is not available, these models offer an appropriate alternative for the Zysset–Curnier model. The isotropic model, which is only based on bone volume fraction, provided inferior results for all regions (mean total norm error 43%). The total norm errors

for the different morphology–elasticity models are illustrated in Fig. 4. When comparing the total norm error and the model norm error, it can be seen that the orthotropy assumption has only a small impact on the errors made by the morphology–elasticity relationships. The full anisotropic stiffness tensor of an arbitrary bone cube and the stiffness tensors computed by the different models are illustrated in Fig. 3.

In the distal radius, the anatomical site with the highest trabecular orientation (highest mean DA), incorporation of fabric information, decreased the total norm error at least by a factor of 2 (see Fig. 4). This highlights the importance of anisotropic elasticity models especially for regions with distinct trabecular orientation.

Using ANCOVA, the dependency of the fabric–elasticity parameters on the anatomical regions was investigated for the Zysset–Curnier model. The regression lines for the models using anatomy-specific parameters were significantly different from those using the parameters from the combined data set (see Fig. 2). However, compared to the anatomy-specific models, the increase in total norm error for models using combined parameters was on average 7.57% higher. This indicates that the fabric–elasticity relationship for the femur, radius and vertebra is significantly but only slightly different.

It is worth mentioning that the bone volume fraction range in the different locations was not similar. This also contributes to the slightly different fabric–elasticity relationship parameters in the different regions.

One limitation of this study is the usage of kinematic boundary conditions. In Pahr et al. (2012), it was shown that kinematic boundary conditions tend to overestimate the effective stiffness of trabecular bone. Therefore, the presented model parameters can be seen as an upper bound, and down scaling is necessary for homogenized FE models.

For modeling of the bone tissue, it was assumed that the heterogeneity of the tissue has only a minor influence on the apparent elastic properties. This assumption is supported by a recent SR $\mu$ CT-based finite element study (Gross et al. 2012).

Mechanical anisotropy of the bone tissue might also have an impact on the apparent elastic behavior. However, since

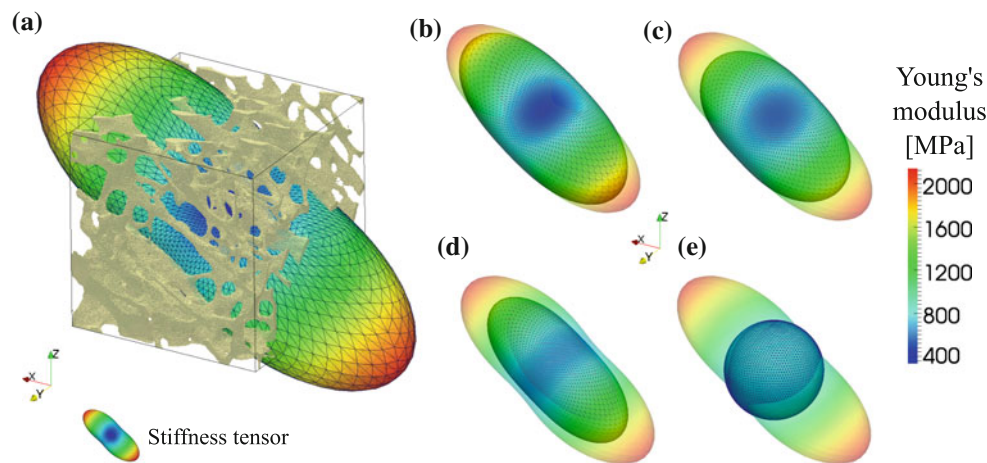


**Fig. 3** **a** Voxel model of an arbitrary bone cube and stiffness plot of the full original stiffness tensor; **b–e** full original stiffness tensor in the background and stiffness tensor computed by **b** Zysset–Curnier, **c** constant orthotropy, **d** constant transverse isotropy and **e** isotropic model in the foreground

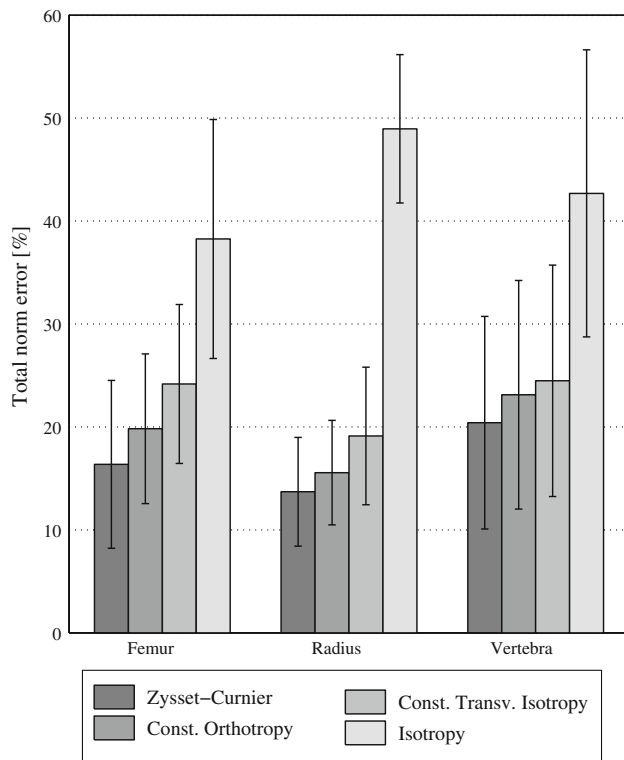


**Fig. 4** Mean total norm errors and standard deviations for femur, radius and vertebra models using different morphology–elasticity relationships

the predominant loading mode of the trabeculae is either compression or bending, isotropic modeling of the tissue with the longitudinal Young's modulus is not supposed to induce considerable errors.

In conclusion, different morphology-based elasticity models were investigated and calibrated using 701 trabecular

bone samples. The presented models can be used to predict the apparent elastic behavior of trabecular bone regions by measuring bone volume fraction and full, limited or no fabric information via CT or MRI. In an indirect way, this may improve clinically relevant homogenized FE models used for the diagnosis of bone quality and fracture risk.

**Acknowledgments** The authors would like to acknowledge Drs. P. Varga, M. Charlebois and E. Dall'Ara for sharing the bone biopsy data.

## References

- Arbenz P, van Lenthe G, Mennel U, Muller R, Sala M (2008) A scalable multi-level preconditioner for matrix-free  $\mu$ -finite element analysis of human bone structures. *Int J Numer Methods Eng* 73(7):927–947
- Bougherara H, Zdero R, Mahboob Z, Dubov A, Shah S, Schemitsch EH (2010) The biomechanics of a validated finite element model of stress shielding in a novel hybrid total knee replacement. *Proc Inst Mech Eng H* 224(10):1209–1219
- Charlebois M, Pretterklieber M, Zysset PK (2010) The role of fabric in the large strain compressive behavior of human trabecular bone. *J Biomech Eng* 132(12):121006.1–121006.10
- Chevalier Y, Pahr D, Allmer H, Charlebois M, Zysset P (2007) Validation of a voxel-based fe method for prediction of the uniaxial apparent modulus of human trabecular bone using macroscopic mechanical tests and nanoindentation. *J Biomech* 40(15):3333–3340
- Chevalier Y, Quek E, Borah B, Gross G, Stewart J, Lang T, Zysset P (2010) Biomechanical effects of teriparatide in women with osteoporosis treated previously with alendronate and risendronate: results from quantitative computed tomography-based finite element analysis of the vertebral body. *Bone* 46(1):41–48
- Cowin SC (1985) The relationship between the elasticity tensor and the fabric tensor. *Mech Mater* 4(2):137–147
- Cristofolini L, Schileo E, Juszczyk M, Taddei F, Martelli S, Viceconti M (2010) Mechanical testing of bones: the positive synergy of finite element models and in vitro experiments. *Philos Trans A Math Phys Eng Sci* 368(1920):2725–2763

- Curnier A, He QC, Zysset P (1994) Conewise linear elastic materials. *J Elast* 37:1–38
- Gibson L (1985) The mechanical behaviour of cancellous bone. *J Biomech* 18(5):317–328
- Goulet R, Goldstein S, Ciarelli M, Kuhn J, Brown M, Feldkamp L (1994) The relationship between the structural and orthogonal compressive properties of trabecular bone. *J Biomech* 27(4):375–389
- Graeff C, Timm W, Nickelsen TN, Farrerons J, Marin F, Barker C, Gluer CC (2007) Monitoring teriparatide-associated changes in vertebral microstructure by high-resolution CT in vivo: results from the EUROFORs study. *J Bone Miner Res* 2007(22):1426–1433 (*J Bone Miner Res* 22914261433)
- Gross T, Pahr DH, Peyrin F, Zysset PK (2012) Mineral heterogeneity has a minor influence on the apparent elastic properties of human cancellous bone: a SR $\mu$ CT-based finite element study. *Comput Methods Biomech Biomed Eng* <http://dx.doi.org/10.1080/10255842.2011.581236>
- Harrigan TP, Jasty M, Mann RW, Harris WH (1988) Limitations of the continuum assumption in cancellous bone. *J Biomech* 21(4):269–275
- Hildebrand T, Laib A, Muller R, Dequeker J, Ruegsegger P (1999) Direct three-dimensional morphometric analysis of human cancellous bone: microstructural data from spine, femur, iliac crest, and calcaneus. *J Bone Miner Res* 14(7):1167–1174
- Hipp JA, Jansujwicz A, Simmons CA, Snyder BD (1996) Trabecular bone morphology from micro-magnetic resonance imaging. *J Bone Miner Res* 11(2):286–292
- Hollister S (1994) A homogenization sampling procedure for calculating trabecular bone effective stiffness and tissue level stress. *J Biomech* 27(4):433–444
- Jones AC, Wilcox RK (2008) Finite element analysis of the spine: towards a framework of verification, validation and sensitivity analysis. *Med Eng Phys* 30(10):1287–1304
- Kabel J, Van Rietbergen B, Odgaard A, Huiskes R (1999) Constitutive relationships of fabric, density, and elastic properties in cancellous bone architecture. *Bone* 25(4):481–486
- Keyak J, Sigurdsson S, Karlsdottir G, Oskarsdottir D, Sigmarsdottir A, Zhao S, Kornak J, Harris T, Sigurdsson G, Jonsson B, Siggeirsdottir K, Eiriksdottir G, Gudnason V, Lang T (2011) Male-female differences in the association between incident hip fracture and proximal femoral strength: a finite element analysis study. *Bone* 84(6):1239–1245
- Mulder L, van Rietbergen B, Noordhoek N, Ito K (2012) Determination of vertebral and femoral trabecular morphology and stiffness using a flat-panel C-arm-based CT approach. *Bone* 50(1):200–208
- Odgaard A, Andersen K, Melsen F, Gundersen HJG (1990) A direct method for fast three-dimensional serial reconstruction. *J Microsc* 159(3):335–342
- Pahr D, Zysset P (2008) Influence of boundary conditions on computed apparent elastic properties of cancellous bone. *Biomech Model Mechanobiol* 7(6):463–476
- Pahr D, Zysset P (2009) A comparison of enhanced continuum FE with micro FE models of human vertebral bodies. *J Biomech* 42(4):455–462
- Pahr DH, Dall'ara E, Varga P, Zysset PK (2012) HR-pQCT-based homogenised finite element models provide quantitative predictions of experimental vertebral body stiffness and strength with the same accuracy as  $\mu$ FE models. *Comput Methods Biomech Biomed Eng* 15(7):711–720
- Roychowdhury A (2009) Application of the finite element method in orthopedic implant design. *J Long-Term Eff Med Implants* 19(1):55–82
- Ruegsegger P, Koller B, Muller R (1996) A microtomographic system for the nondestructive evaluation of bone architecture. *Calcif Tissue Int* 58(1):24–29
- Silva MJ, Keaveny TM, Hayes WC (1998) Computed tomography-based finite element analysis predicts failure loads and fracture patterns for vertebral sections. *J Orthop Res* 16(3):300–308
- Taddei F, Cristofolini L, Martelli S, Gill H, Viceconti M (2006) Subject-specific finite element models of long bones: An in vitro evaluation of the overall accuracy. *J Biomech* 39(13):2457–2467
- Turner CH, Cowin SC, Rho JY, Ashman RB, Rice JC (1990) The fabric dependence of the orthotropic elastic constants of cancellous bone. *J Biomech* 23(6):549–561
- Varga P, Dall'Ara E, Pahr DH, Pretterklieber M, Zysset PK (2011) Validation of an hr-pqct-based homogenized finite element approach using mechanical testing of ultra-distal radius sections. *Biomech Model Mechanobiol* 10(4):431–444
- Varga P, Zysset PK (2009) Assessment of volume fraction and fabric in the distal radius using hr-pqct. *Bone* 45(5):909–917
- Whitehouse WJ (1974) The quantitative morphology of anisotropic trabecular bone. *J Microsc* 101(Pt2):153–168
- Wolfram U, Wilke HJ, Zysset P (2010) Valid  $\mu$  finite element models of vertebral trabecular bone can be obtained using tissue properties measured with nanoindentation under wet conditions. *J Biomech* 43(9):1731–1737
- Zysset P (2003) A review of morphology–elasticity relationships in human trabecular bone: theories and experiments. *J Biomech* 36(10):1469–1485
- Zysset P, Edward Guo X, Edward Hoffler C, Moore K, Goldstein S (1999) Elastic modulus and hardness of cortical and trabecular bone lamellae measured by nanoindentation in the human femur. *J Biomech* 32(10):1005–1012